J. Sound Vib. (1966) 3 (3), 422-444

THE NATURE OF LIMITATIONS IMPOSED ON THE PERFORMANCE OF A HELICOPTER ROTOR

J. M. HARRISON AND J. B. OLLERHEAD

Westland Aircraft Limited, Yeovil, Somerset, England

(*Received* 30 *May* 1965)

A systematic theoretical approach to the investigation of helicopter rotor performance limitations is outlined. The essence of the method is a digital computer programme devised to solve the equations of motion of a typical articulated blade, part of a rotor system in a state of steady flight. This solution is the starting point from which the detailed rotor performance is calculated, a process which involves, in addition to the main performance programme, an interrelated system, the whole forming a hierarchy. Each member programme is designed for a particular function and the flow of data is routed according to the required form of output. The main programme and the next in order of importance, computing downwash distribution in the rotor disc plane from a knowledge of blade loading and wake geometry, are described in some detail along with their mathematical models. A brief history of development of the method precedes a formal comparison of computed output and experimental data. Some indication is given of refinements introduced during this stage. Detailed discussion is restricted to downwash distribution and its effects, first upon blade bending stresses. An interpretation of the mechanism modifying power requirements follows, and is combined with further description of an attempt to reconcile blade loading and downwash distribution in a consistent blade motion solution. It is shown how, by linking four programmes in a closed loop, rapid progress is made towards convergence.

INTRODUCTION

From the early days of helicopter development it has been recognized that, over a substantial part of the flight envelope, energy availability is far from being the sole criterion for determining performance boundaries. In particular, a typical rotor shows a marked reluctance, at the high speed end of the range, to turn a steady supply of power into translation, with any concessions towards the physical comfort of vehicle occupants or the well-being of mechanical components, even though the power plant may be purring smugly well within its capabilities. A solution to this problem lies not in mere harmonization of rotor geometry, because the same rotor might well convert, imperturbably, the last foot pound per second wrung from a straining engine, into a smooth towering ascent. One accepted long term approach to an understanding of the nature of this problem lies in the critical examination of the dynamic response of a rotor system to external excitation, predominantly aerodynamic. We have undertaken a comprehensive investigation along these lines and currently it is well advanced. The method is basically theoretical, involving the construction of mathematical models to represent the motion of a typical rotor blade within its environment. Related digital computer programmes have been written to effect the necessary calculations. The underlying philosophy has been dictated to a large extent by the tools available, in the first instance a comparatively slow computer with a limited amount of core store and no backing store. More recently, the available core store has been doubled, rendering feasible the refinement and elaboration of the original models.

A start was made with the simplest representative dynamic model, a rigid blade articulated in flapping. This apart, few concessions were made, and the original aerodynamic model was as realistic as available data allowed although, in the formative stages, downwash distribution was deliberately linearized. From this foundation, a hierarchy of related computer programmes is being gradually assembled, so devised that every known aspect of performance limitation can be investigated, either in isolation or in combination, using the simplest acceptable model. To aid in identifying the appropriate model, the operational programmes have been subject to verification at each stage of development, by comparing their output with available test data, from more than one source if possible. The investigation, though well advanced, is far from complete and discussion will be restricted to two important sources of trouble, non-uniformity of downwash distribution in the rotor disc plane, and blade flexibility in flatwise bending.

COMPUTATION OF BLADE MOTION

At the heart of the hierarchical system of computer programmes to be described later lies the "performance" programme. Its primary function is the solution of the blade equations of motion, but a comprehensive range of performance data is an important by-product, hence the name. The technique may be familiar to some, but a description is appropriate, not merely for the benefit of the uninitiated, but also to introduce the method as a whole and the underlying philosophy. Each solution is particular and relates to a state of steady flight, not necessarily rectilinear, the flight configuration being defined by a sufficient number of parameters. Apart from rotor geometry and dynamic characteristics, these are principally a blade pitch distribution, as constrained by the flight controls, shaft incidence, incident velocity, rotor tip speed, and ambient enthalpy. In steady flight it is readily apparent that blade motion would repeat over successive revolutions, and the approach adopted is a step by step technique using numerical integration, with a test for convergence at the end of each revolution. This latter starts logically enough at zero azimuth from a suitable initial state, and is best understood in terms of the simplest model, referred to earlier.

Angle of attack distribution is calculated at a number of specified reference points along the blade, as illustrated in Figure 1. Lift and drag coefficients determined as functions of angle of attack and Mach number are then resolved in terms of flapping and lagging, and the process is repeated at each radial station until the whole blade has been treated. Then, integrating along the effective length of the blade, the aerodynamic flapping moment is evaluated and substituted in the equation of motion to produce in turn a flapping acceleration. Integration of other forces and moments required later is conveniently dealt with at this point. Two successive integrations made over a small interval of time, which at constant rotor speed is interpreted as an equivalent azimuth interval, lead to new values of flapping velocity and displacement appropriate to the next azimuth station.

Meanwhile other changes have taken place under constraint, affecting blade pitch and incident velocity vector, and all contribute to a new angle of attack distribution. The azimuth cycle starts anew at this point and the process continues until a rotor revolution is complete, whereupon, blade flapping displacement is compared at selected stations with the equivalent history of the preceding revolution. Upon attainment of convergence, taking as few as three revolutions, but varying according to flight configuration and model complexity, accumulated data is organized into output according to specification. In the particular case described, a typical format would comprise a radial distribution of normal and tangential force coefficients, angle of attack, the in-plane component of incident velocity and downwash normalized with respect to tip speed and, in the former case, as

Mach numbers. Each sub-table relating to an azimuth station would terminate with the integrated value of relevant force and moment (or torque) coefficients. The flapping angle distribution is describable as a history or a Fourier series, the latter acting as an indicator of potential vibration amplitudes. The lists would be rounded off with the integrated rotor lift, drag and power required components, plus relevant data identifying the flight case.

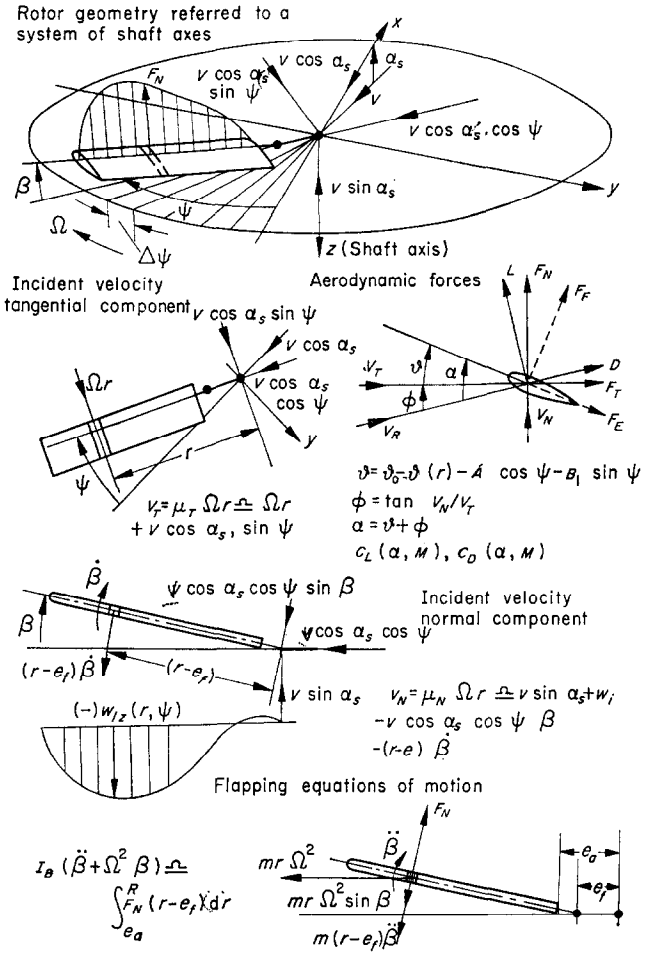

Figure 1. Rotor geometry, blade aerodynamics and flapping dynamics. †

The power of such a method should be immediately apparent for not only is the gross performance computed in tangible form, but also the detailed behaviour of the blade according to its instantaneous location. Examination of traditional blade stall and drag divergence criteria are facilitated, and critical areas are revealed. The basic method has much greater potential however and the extension to more ambitious models is rewarding. Admission of lagging, although fairly straightforward, poses some problems but yields in return a first approximation to the residual exciting forces at the rotor hub, forces which are an important source of body vibration. On the other hand, the treatment of a flexible blade, which was necessary, in the first instance, for calculating bending stresses, proved to be troublesome and success was elusive. After several abortive attempts

† A list of definitions of symbols is given in the Appendix.

involving mass/spring models, all wasteful of computer time and storage, an elegant and economical technique was evolved, following a suggestion by Dr. J. P. Jones.

Blade flexible motion is described in terms of normal modes, a concept found to match our philosophy perfectly, for it allows the basic data describing blade motion to be derived using a separate independent programme, and thereby effectively extends the power and capacity of the computer. A multi-degree of freedom primary representation generates a secondary model, one capable of describing adequately the motion of the blade in as little as three degrees of freedom. Moreover, the blade shape, being defined as the sum of a series of continuous functions, allows the introduction of aerodynamic coupling with ease and economy (Figure 2). Because the modes are orthogonal, these are to a first

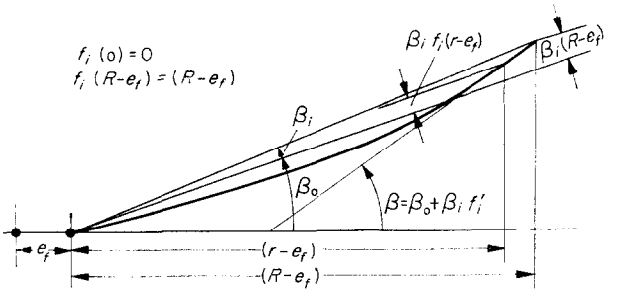

Figure 2. Normal mode representation of a flexible blade in transverse bending. In general, treating rigid flapping as a zeroth mode where in $f_0(r-e_f) = (r-e_f)$, $f_0'(r-e_f) = 1$, then $\beta = \sum_{i=0}^{n} \beta_i f_i'$, and the modes are coupled aerodynamically through the normal component of incident velocity,

$$V_N \simeq V\sin\alpha_s + w_{i_s} - V\cos\alpha_s\cos\phi \sum_{i=0}^{n} \beta_i f_i' - \sum_{i=0}^{n} \dot{\beta}_i f_i.$$

For bending about a principal axis, it can be shown (1) that the equation of motion for the ith mode,neglecting some low-order terms, approximates to

$$\ddot{\beta}_i \int_{e_f}^{R} m f_i^2 \,dr + \beta_i \left[\Omega^2 \int_{e_f}^{R} mr \int_{e_f}^{r} (f')^2 \,dr\,dr + \int_{e_f}^{R} EI_{\beta\beta}(f'')^2 \,dr \right] \simeq \int_{e_a}^{R} F_N f_i dr.$$

In the process of deriving the secondary from the primary model only the mode shapes and their derivatives emerge discretely along with the associated natural frequencies and it is convenient to recast the equations non-dimensionally in the form:

$$\frac{\ddot{\beta}_i}{\Omega^2} + \omega_i^2 \beta_i \simeq \frac{\gamma_i}{2a}\left(\frac{C_M}{s}\right).$$

approximation the only couplings and, occurring as they do in the aerodynamic terms which are treated as forcing functions, the model reduces ultimately to a system of virtually independent equations (1), the greatest economy of all. There is of course the inevitable compensating disadvantage. Each mode is associated with a natural frequency, and ill-conditioning tends to show itself as a residual oscillation at that frequency. In practice it has been found necessary to integrate using a fourth order Runge-Kutta routine associated with a 10° interval to achieve satisfactory solutions in the higher modes.

Although the expansion to the ultimate model is a logical path to explore, it is not the only one. A typical modern metal helicopter blade is comparatively stiff edgewise and in torsion. It is therefore intuitively evident that a good first approximation to blade stresses and control loads could be sought using a model with only flatwise bending admitted, and we are actively pursuing such a policy. It is our intention to compute control

loads in the first instance using an auxiliary programme accepting output from the appropriate main rotor performance programme so restricted. Computation of comprehensive performance in one fully representative programme using a larger computer follows logically but at a later stage, and requires extension to the aerodynamic as well as the dynamic model.

One of the more important aerodynamic influences, downwash distribution, has yet received only passing mention. Linear representation, with uniform longitudinal gradient, is adequate for computing energy performance. Actual distribution is however characterized by appreciable higher harmonic content which affects significantly blade load grading and thereby elastic deformation, as will be demonstrated later. Computation of a realistic distribution is a formidable problem requiring the full power of the computer for its treatment, thus meriting a separate auxiliary programme. As Figure 1 shows, the local downwash component is an important constituent of the aerodynamic force pattern, affecting blade motion, and a consistent solution can be achieved only if its evaluation is included as part of an iterative macro-loop. Since both major programmes involved effectively fill the core store currently available, a segmentation technique has to be used. Operation without backing store is perforce manual, but is no disadvantage during a research phase since it is necessary to appraise critically the output at each stage. Actually, as is shown later (Figure 7), more than two programme segments are involved and the construction of a fully automatic loop entails much preparatory work. Such a loop would of course be economically viable only on a large high speed computer preferably with direct access backing store.

DOWNWASH MODEL

Our fundamental philosophy is two-pronged: first, break the problem up into parts capable of being dealt with in sequence using limited computing facilities; then describe each system or sub-system in terms of the simplest realistic model. Downwash distribution is an example where simplicity might even pay off handsomely, facilitating the achievement of clearer insight; nor does additional complexity necessarily result in more realistic representation. In the event we have progressed no further than an elaboration of the simplest basic model, adapted from reference (2), to suit our needs. This technique involves the building of a model in two stages and is illustrated in Figures 3 and 5.

In the first stage, the wake is represented as sets, one per blade, of discrete trailing vortex filaments, each filament issuing from a designated radial station. The system is referred to Cartesian co-ordinates, originating at a point in space occupied by the rotor centre when the reference blade is downwind instantaneously at azimuth zero. The blade tip paths are described in the xy-plane. It is assumed for simplicity that there is no distortion of the wake parallel to that plane so that, viewed along the z-axis, it appears as a regular pattern of stationary trochoidal filaments growing uniformly along the x-axis. Transport parallel to the z-axis is semi-rigid in that each element is assumed independent of its neighbours but carried at uniform velocity. The rate is equivalent to the normal component of incident velocity pertaining at the instant of generation. Distance transported relative to a reference blade element is thus proportional to the "wake age" parameter.

Downwash distribution can be integrated directly from such a model but would involve much computing effort. Advantage can however be taken of the law governing the field induced by a line vortex. Recognizing that adjacent portions of filaments are dominant, it is feasible to neglect their curvature and substitute a rectilinear wake model. It is readily seen that the orientation of the filaments constituting such a system is constantly changing

and depends instantaneously on the reference blade azimuth, amongst other parameters. By referring to the projection in the xy-plane, each replacement filament is defined as tangential to a trochoidal filament at a point where the latter intersects the reference blade or its extension. An implication is that, when re-entrant, a curved filament is replaced by two or more rectilinear filaments. To simplify computation, these latter are treated as near wake, semi-infinite filaments attached to the reference blade, or far wake, infinite filaments relating to another blade or to a re-entrant loop from the reference blade.

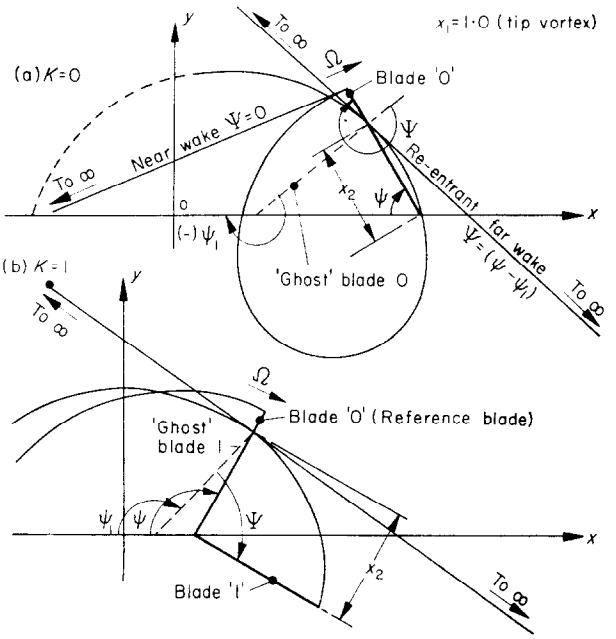

Figure 3. Wake representation for a four-blade rotor ($b=4$).
Blade element co-ordinates are stated parametrically as

$$x = \mu_x\left(\frac{2\pi\kappa}{b}+\psi\right)-X\cos\psi, \quad y = X\sin\psi.$$

The intersection of the reference blade (station ψ_2) and the projection on the tip-path plane of the trochoidal filament is given by $X_2\cos\psi = X_1\cos\psi_1+\mu_x\Psi$ and $X_2\sin\psi = X_1\sin\psi_1$.

$$\Psi = \frac{2\pi\kappa}{b}-(\psi_1-\psi)$$

is a parameter defining the age of the filament element. $\Psi = 0$ defines a near wake filament.

In effecting the solution of the intersection, an elegant and ingenious method was devised by a colleague, L. H. Wilkes (see Figure 4). The sequence is in two parts, first iterating for the wake-age parameter. Later, substitution is made for the radial intersection coordinate. The process is completed by calculating the actual downwash distribution. It is of course recognizable that of the radially disposed filaments in the first stage model, only those at the blade extremities would be physically discrete. The intermediate pattern represents a vortex sheet. Only trailing vorticity is represented directly. Shed vorticity can be implied, within the model limitations, by ascribing to each trailing filament a strength appropriate to radial circulation gradient at the point of issue. Where there is no

intersection of blade axis and filament projection, special provision would be necessary to idealize the wake. Trial calculations show however that, as the blade passes through the boundary of determinate solutions, the influence of the appropriate loop fades rapidly with increasing azimuth. This ready made criterion has been accepted provisionally. Reconciling realism with economy, the current computing cycle is terminated, and the next initiated.

The downwash distribution as computed using this model cannot be applied directly in its raw state either to the computation of blade motion or of wake transport. In the first instance it is most unlikely that a choice of reference stations common to both programmes is feasible. In the second it is in general necessary to interpolate for non-integral values of

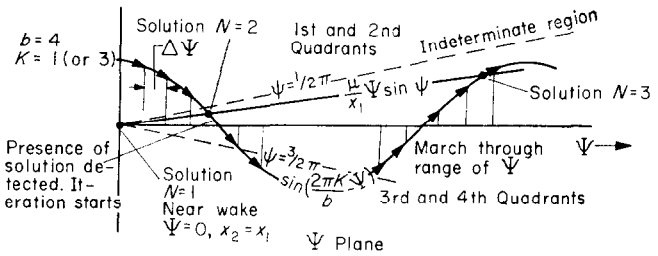

Figure 4. Determination of idealized wake geometry. The first part of the solution is effected in the Ψ plane, recasting the equations of intersection

$$o = X_1 \sin\left(\frac{2\pi\kappa}{b} - \Psi\right) - \mu_x \Psi \sin\psi, \tag{1}$$

$$X_2 = X_1 \cos\left(\frac{2\pi\kappa}{b} - \Psi\right) + \mu_x \Psi \cos\psi. \tag{2}$$

(1) is solved by iteration, increasing Ψ by increments. The value of Ψ thus arrived at is substituted in (2) for X_2. Several important advantages accrue using this method: (i) the number of solutions is halved since for every value of ψ in the 1st and 3rd quadrants there is a corresponding solution in, respectively, the 2nd and 4th quadrants; (ii) including the near wake, there are a maximum of three solutions in each wake spiral, not all necessarily determinate; having reached a condition of non-determinacy in the case of a particular solution there is then no need to pursue that solution further over the remainder of the quadrant; (iii) the danger of omitting, duplicating or misplacing solutions is obviated; (iv) by restricting the range of Ψ in which solutions are sought wake decay can be simulated, and the age or length of effective wake readily controlled.

the "ghost" blade azimuth (the appellation "ghost" being most readily understood by reference to Figure 3). At first sight no great problem is presented since interpolation from tabulated data is a straightforward process amenable to programming. There is however special significance in the epithet "raw", as used in the first sentence of this paragraph. In practice it is quite possible for a blade to cut through a vortex core and be subjected to large localized downwash gradients. It is also possible to compute such states using an idealized model but not with any great confidence that the results will be representative. On the grounds that it would be safer to abjure such conditions a safeguard was built into the programme which effectively eliminates infinities but still allows generation of large saw-tooth peaks. The erosion of these is left to an ancilliary process perhaps best described as double-smoothing. Working in terms of the azimuth, a harmonic analysis is made at each radial station. Polynomials are then fitted, one per set of Fourier coefficients. Thus each local downwash value is influenced by the rest, predominantly by its neighbours. Not only are the original rugged contours softened, but the downwash value can be

quickly determined for any point on the rotor disc. Since several hundred such values are required during each azimuth cycle, curve fitting is a compromise between fit and economy. During the verification phase a sextic six harmonic combination has been chosen provisionally.

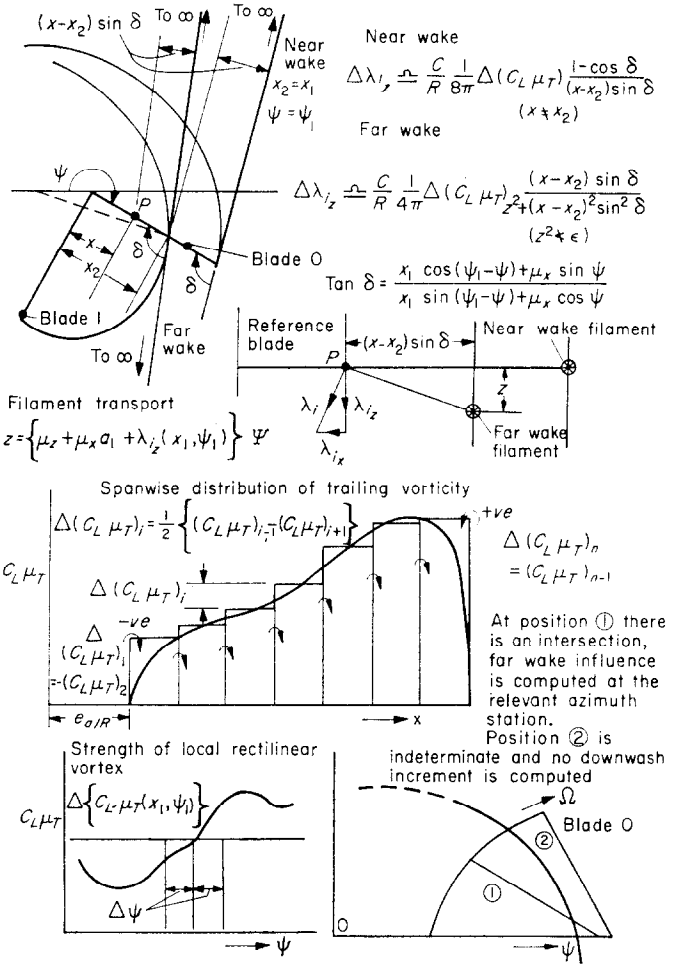

Figure 5. Computation of downwash distribution.

HIERARCHY OF PROGRAMMES

As was indicated earlier, the heart of the system is the rotor performance programme as a member of a hierarchy. The place of a programme in that hierarchy is defined in terms of the number of degrees of freedom admitted and the output format. The latter is to a great extent specified by the model but not entirely. The basic flow diagram is illustrated in Figure 6 and embraces models of articulated rotors in one or more degrees of freedom. The technique is readily adaptable to deal with non-articulated rotors, which are, however, considered beyond the scope of this paper. Flapping, since it is the dominant agent through which aerodynamic coupling is transmitted, is a mandatory degree of freedom and the others may be admitted in suitable combination covering lagging and flatwise and edgewise bending. For lucidity of presentation, provision for torsion is not shown. Programmes are segmented for ease of assembly, as shown diagramatically, and

each segment is logically replaceable as a unit. A typical example is the aerodynamic segment computing lift and drag coefficients according to the specified aerofoil section. Some segments are further subdivided into modules either because they are large or because the modules are common to all programmes. As can be seen, the first segment is

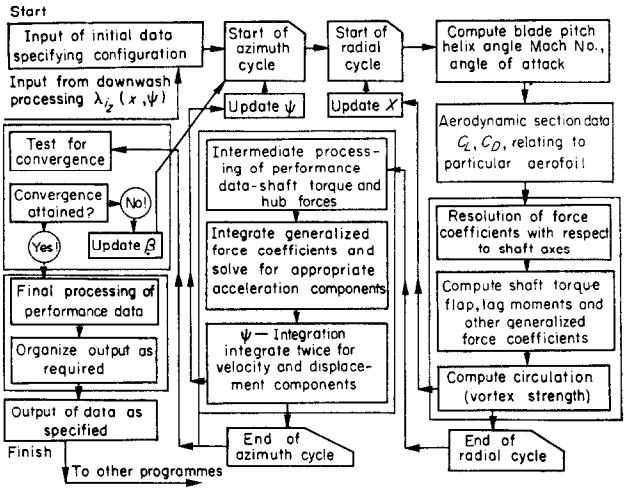

Figure 6. Basic rotor performance programme flow diagram.

concerned solely with input. The second computes angle of attack and Mach number, both necessary to evaluate the force coefficients in the third. The fourth, amongst other operations, resolves these coefficients in a form suitable for substitution in the blade equations of motion, which are solved, with the solutions being integrated twice in the

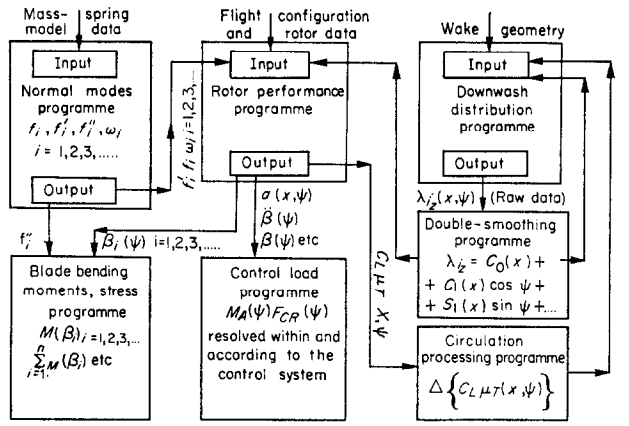

Figure 7. Relationship between programmes within hierarchy.

next segment. The convergence check, pre-output and output segments follow in that order.

Only slightly less important as members of the hierarchy are the bigger auxiliary programmes used for post-output processing. Typical examples are those for computing blade stresses and control loads; but perhaps the most important, and certainly the most complicated, is the downwash distribution programme. The technique involved has

already been accorded some description and for completeness a flow diagram (Figure 8) shows in greater detail some of the intermediate processes. Of possible interest is the method of detecting the number of determinate solutions in the chosen range of wake age. Cycling by small increments of that parameter, a change of sign in (1) of Figure 4 indicates the presence of a solution which is then readily and rapidly enumerable using Newton's method. Effort is thus not wasted on attempting to evaluate indeterminate solutions. The

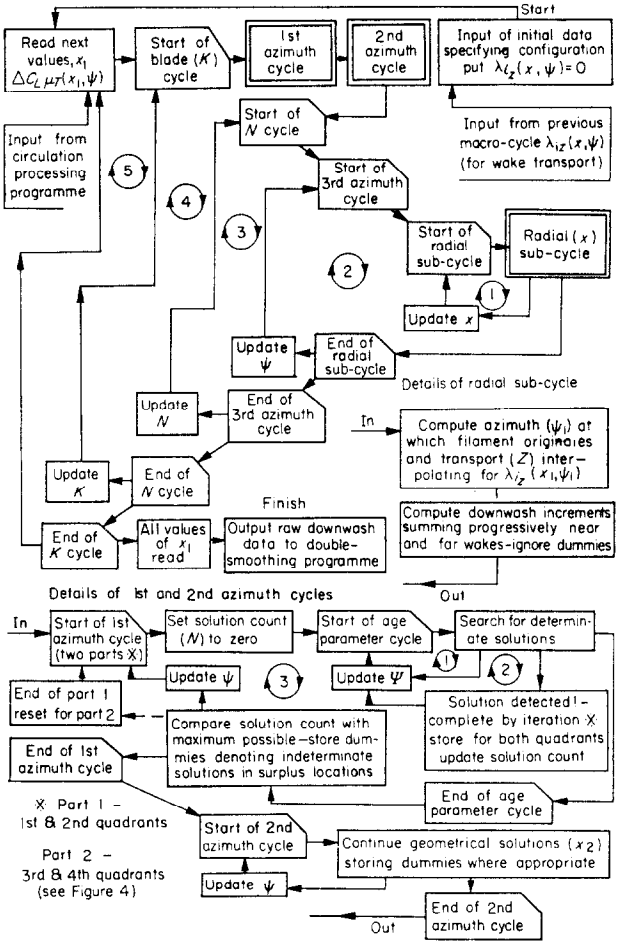

Figure 8. Downwash distribution flow diagram.

downwash programme links up with a special series of performance programmes in an iterative cycle to achieve consistent blade motion solutions. The series is special only in the sense that the pre-output and output segments are modified to produce data in a format acceptable by a further intermediate auxiliary programme designed to interpret the circulation distribution as a "staircase" (Figure 5), singly smooth the steps in terms of the azimuth, and re-present the data in tabular form. In turn the output of the downwash programme is doubly smoothed as described previously by yet a further auxiliary programme, and this data is then available as input for both performance and downwash distribution programmes, in the latter case for computation of the wake transport normal to the tip path plane. Figure 7 depicts the flow of information in this and other instances.

APPLICATION OF METHOD AND COMPARISON WITH TEST RESULTS

Before submitting the output of the performance programmes to the test of comparison with measured data, a rigorous programme of development was carried out to ensure that conditioning was adequate to cope with all physically feasible flight configurations. For this purpose, a simple Glauert downwash distribution with linear longitudinal gradient was adopted. Only after confidence in the programme had been established was an attempt made to examine the effects of non-uniform downwash. In the early stages of the programme development phase a typical cruise case was treated. Admitting only one rigid, flapping mode, a simple method of numerical integration was

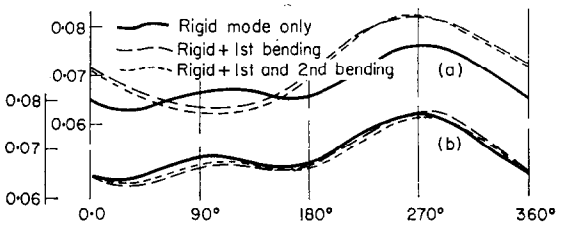

Figure 9. (a) Non-dimensional tip displacement; (b) rigid mode amplitude.

found to be satisfactory, but with the introduction of higher modes difficulty in attaining convergence was experienced and resort was made to more elaborate techniques, culminating in the application of a fourth order Runge-Kutta routine. To aid in conditioning and to simulate structural damping, a nominal 2% of critical damping was entered for each elastic mode. In parallel with this effort, a critical assessment was made of the minimum number of normal modes needed to simulate blade motion realistically in

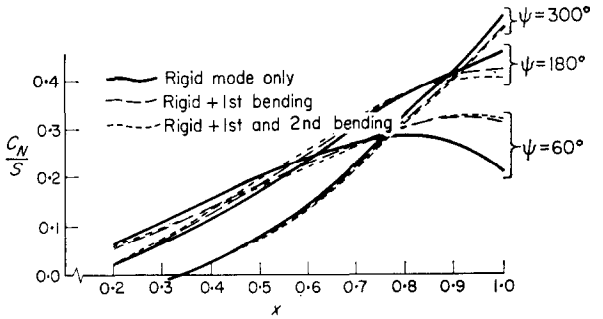

Figure 10. Effect of elastic modes upon normal force coefficient.

flatwise bending. Each mode was released in succession up to and including the third. The computed amplitude of this latter is too small to show in Figure 9, being of the order of a pencil line thickness. The flapping angle, defined in Figure 2 as, not the root slope, but the datum from which elastic deformation is measured, is seen to be affected only marginally. In consequence, and because even the first mode amplitude is comparatively small, the overall effect upon aerodynamic loading, illustrated in Figure 10, is slight, except locally near the tip in the advancing blade region. Both are points of significance taken into account in justification of assumptions made to simplify interpretation of test data. It was decided provisionally at this stage that three elastic modes constituted adequate representation in flatwise bending. The performance programme, when fully

developed, coped readily with a cruise case, comfortably remote from the starker regions of the flight envelope, and so more strenuous trials were instituted. Running a number of cases in which it was contrived that one mode at a time was at or near resonance, convergence was attained on every occasion within four rotor revolutions. The most testing of the series, illustrated in Figure 11, represents a lightly loaded rotor operating at an advance ratio of 0·7, in near auto-rotational conditions appropriate to a high speed compounded helicopter. The second mode history is shown to exhibit a marked residual at the blade natural frequency 3·97 R.

Downwash in practice is by no means uniformly or linearly distributed over the rotor disc, as is well known, and as the next verification phase of the programme confirmed. The first stage of this phase was to estimate a typical distribution, operating on the data of reference (3), the most comprehensive collection currently available. Even so, interpretation is not entirely straightforward and, in particular, elastic deformation is not presented directly as such but in the form of bending moments at six radial stations,

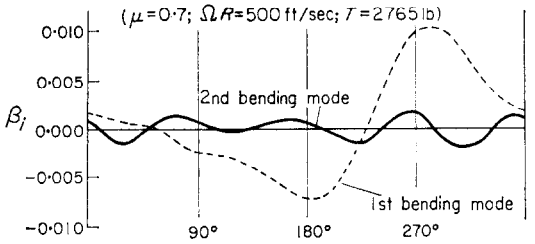

Figure 11. Elastic response in extreme flight configuration.

insufficient to define the blade profile adequately. In face of a far from negligible economic penalty, and with the justification of previous experience, elastic deformation was neglected and the analysis was made on the basis of a rigid blade. It is appropriate at this juncture to comment briefly on the section aerodynamic data used in the performance programme, compiled currently from references (4) and (5), and relating to a N.A.C.A. 0012 aerofoil. Reference (4) covers angles of attack up to a maximum of 15°, and a representative range of Mach numbers, providing data for all but a small area of the rotor disc located in and around the reverse flow region. Continuity in this latter region is provided by reference (5). Although more recently acquired data is available, we have found the original quite satisfactory to date and have felt no compelling need to modify the relevant programme segment. Similar data is of course used when deducing a downwash distribution from a knowledge of flight configuration, blade motion and loading. The technique is straightforward and need not be enlarged upon. Processing is by auxiliary programme, and as an overall check of accuracy, the computed distribution, after double smoothing as described previously, was fed into a rigid blade performance programme along with other data relating to the chosen flight case. The check consists of reproducing blade loading and flapping history. Agreement in this respect has, with some reservations, been close for the few cases so far analysed. A satisfactory comparison is a green light to move to the next stage and, feeding identical data into a performance programme higher in the hierarchy, to compute elastic deformation as represented by the first three normal modes in flatwise bending.

It is here that adequacy of representation is given a further test. Blade motion history channelled through an auxiliary programme (Figure 7) is interpreted as bending moments. Results of a typical case plotted in Figure 12 show that contributions from the third mode are appreciable, contrary to former experience. The reason is not obscure. Although

amplitude shrinks by one order with each successive mode, the magnitude of the mode shape second derivative, on which bending moment depends, has a compensating effect, growing by half-an-order with each mode. It is, debatable, however, as to whether admission of higher modes would modify the output significantly even at resonance. Thus, reverting briefly to the marginal case illustrated in Figure 11, the order of the second mode amplitude at 0·002 is typical, in spite of the strong residual, and remains

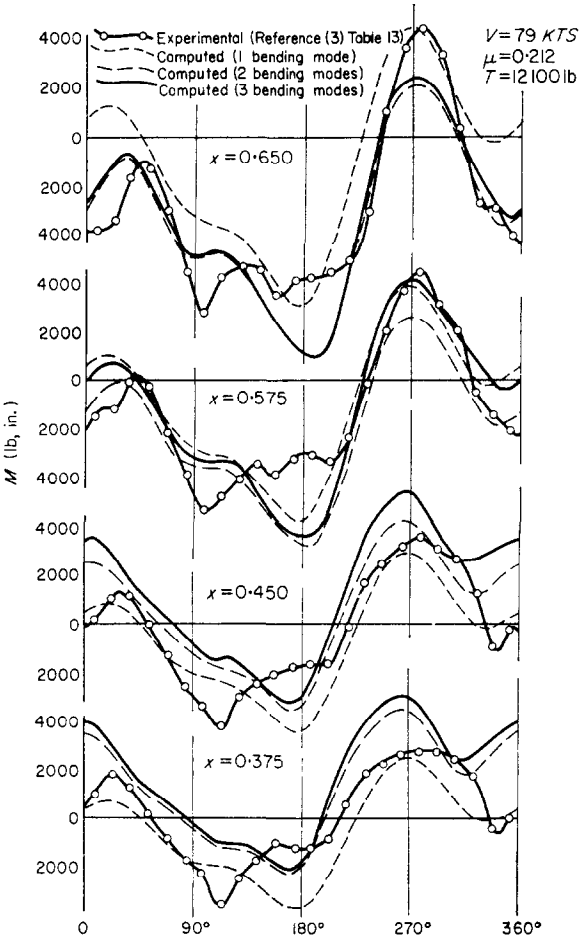

Figure 12. Bending moment distribution.

small compared with the first mode. Moreover, all dominant peaks are evident in the first mode, at least in embryonic form, the second and third modes merely having a modifying influence, the importance of which, incidentally, wanes rapidly in the vicinity of a node. Only the second mode is seen to affect the profile appreciably. The results are inconclusive to the extent that no strain gauge measurements were recorded outboard of station 0·65. Second derivatives of the two higher modes as calculated both have maximum values in the vicinity of station 0·80. Furthermore, as will be explained later, interpretation of the measured data is as yet to only a first approximation. Nevertheless, agreement with experiment admitting only these first three modes is sufficiently good to be described as encouraging.

A mild burst of enthusiasm at this stage was tempered by the sobering thought that the bending moment histories had been produced on a basis of a tailored downwash distribution, and that what had been demonstrated principally was the adequacy of the dynamic model. A more satisfying achievement would be an all-computed case, blade motion, downwash distribution and integrated performance. The question arose as to what extent bending is influenced by the downwash distribution. An answer was sought by running a comparable case wherein the downwash was replaced by one of the original Glauert

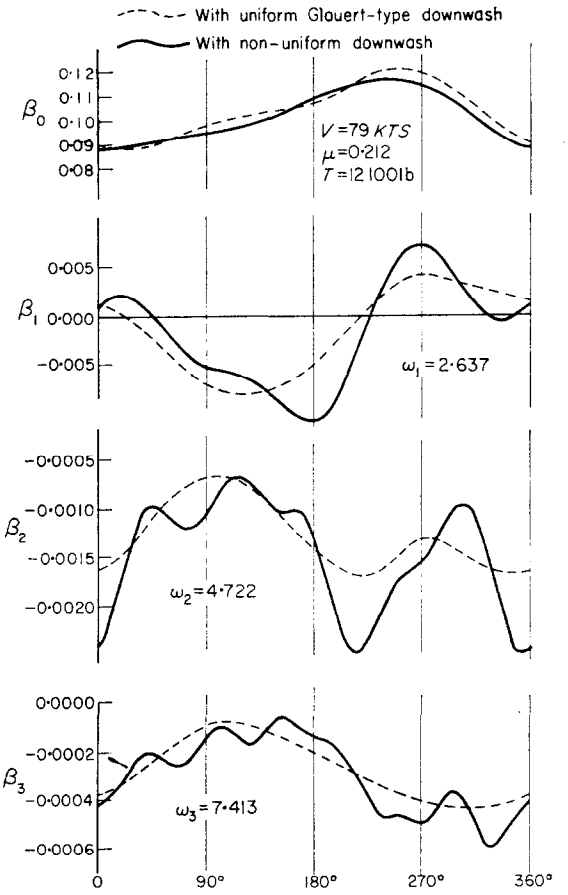

Figure 13. Elastic response to non-uniform downwash.

patterns. Some care was taken to produce equivalent output, particularly in terms of rotor thrust, and even to the extent that flapping histories matched closely as shown in Figure 13. The mode shapes, and thus bending stresses, are seen to be affected profoundly by the harmonic content of the downwash distribution. The original smooth contours have sharpened and, particularly in the higher modes, have become distorted with the appearance of new peaks and troughs. Clearly, blade stresses calculated on a basis of linear downwash distribution would be unrealistic, leading to optimistic estimates of blade life. Two ways of deriving suitable distributions are open. One, already described, relies on the availability of sufficient experimental data to cover a representative flight envelope, but such information would be suspect unless coverage also included a number of aircraft in order to cater for changes in other than the main wake angle parameter. Greater flexibility

would however be conferred if it were possible to compute realistic distributions to order. With this primary aim, a parallel investigation into the subject of rotor wakes was initiated.

Following the philosophy propounded earlier, a downwash model was gradually built up. On the basis of experience, and taking into account computing economy, an azimuthal interval of 15° was chosen and downwash computed at thirteen equally spaced radial stations, coinciding with those used in the performance programme. The equal spacing is not arbitrary, but the result of experimentation. Downwash is not computed at the

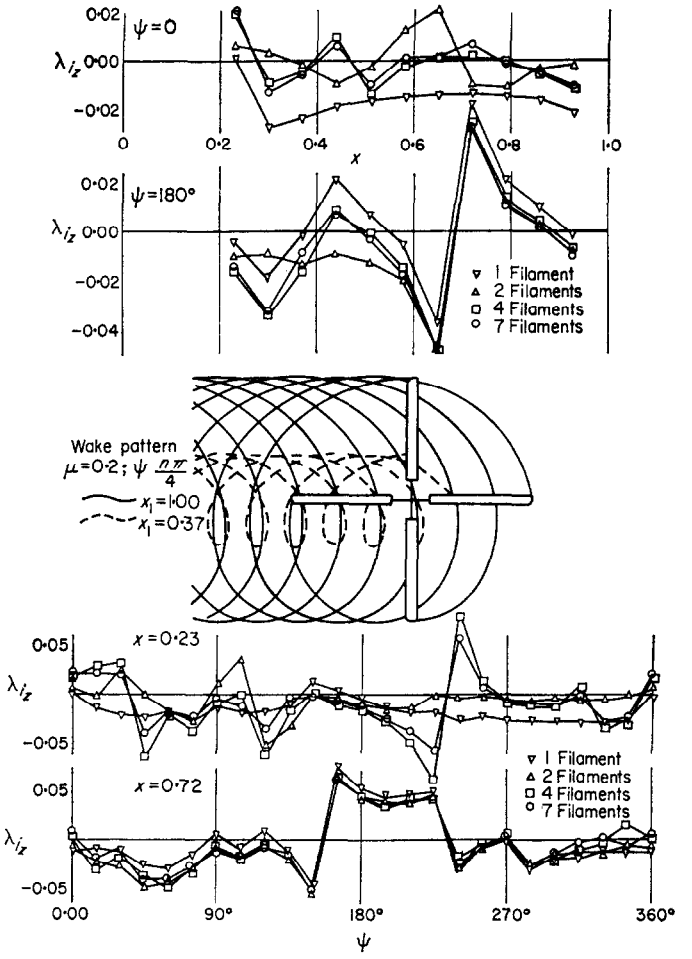

Figure 14. Computed downwash distributions.

extremities, but fixed as a boundary condition of zero circulation. It so happened that twelve equal strips yielded an acceptable radial load grading and a realistic tip loss, as well as being advantageous for the description of mode shapes. Recognizing that the discrete tip vortex must be dominant, the first pattern was based on a single filament issuing from the blade tip. Vortex strength was computed by averaging, around the azimuth, peak values of circulation; these, in practice, always occur towards the tip. Such a model is not of course completely realistic. There must be an associated vortex sheet, rolling up eventually in the root blade region. In the next model roll-up was concentrated in one vortex issuing from station 0·37, chosen after examining the mean circulation profile. Downwash as computed by the two models differs fundamentally, particularly in the

downwind sector. The curves of Figure 14 show the raw data, relating to the two models, at azimuthal stations 0 and 180°. These stations are deliberately chosen as representing the extremes. Examination of the appended wake planform reveals clearly why there is closer agreement in the upwind sector and towards the tip downwind. In these regions the tip vortices are dominant. Downwind in particular, the hash of inboard filaments makes its presence felt. It being clearly necessary to represent the vortex sheet more

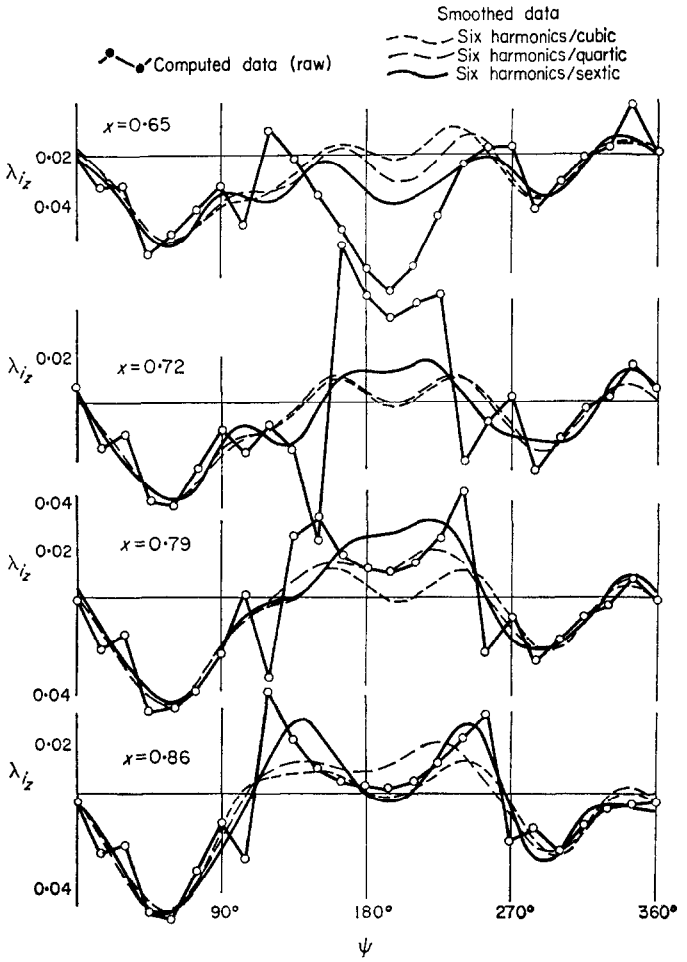

Figure 15. Computed downwash, two-way smoothing.

realistically, a four filament model was tried next, breaking down the inboard vortex into three filaments located at the root station (0·16), 0·37 and 0·58. The hash downwind is even more confused, but the texture is finer. Finally a seven filament model was chosen with an eye to automatic computation of the "staircase" (Figure 5) and involved every other radial station. Correlation between these last two models begins to show. To give a clearer overall picture, azimuthal distributions at stations 0·23 and 0·72 are plotted for the four models. It is as well that the wide differences evident at the inboard station are hardly likely to be significant in terms of blade loading.

First comparisons with test data were made using the seven filament model, and revealed important discrepancies. In an attempt to remedy these, a further refinement was

introduced allowing for variation of circulation around the azimuth. As mentioned before, the effect of shed vorticity is thereby implied, and no attempt has been made to deal with it directly. The computed data used for comparison was in each case doubly smoothed as described in an earlier paragraph. Changes in profile imposed by such smoothing are illustrated in Figure 15 for stations 0·65, 0·72, 0·79 and 0·86. Note in particular how the large gradient between 0·65 and 0·72 in the upwind sector has been ironed out and the double upwash peak gradually introduced at station 0·86. The amount of smoothing is

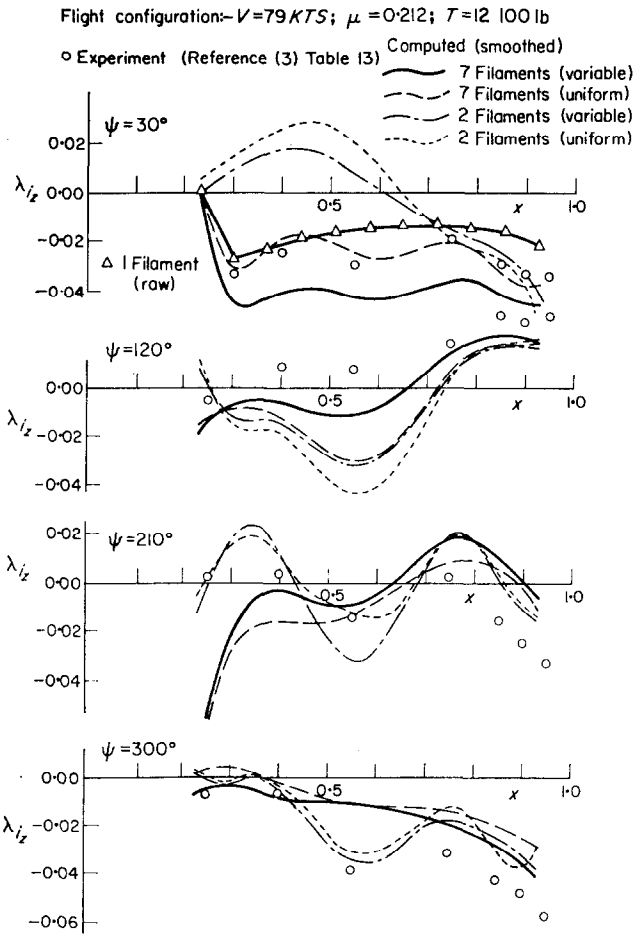

Figure 16. Comparison of theoretical and experimental downwash.

arbitrary, bringing an element of art into the analysis, and must be borne in mind when appraising the curves of Figure 16. These relate on the one hand to downwash as "measured" and on the other, as computed with uniform and variable circulation from models with two and seven filaments.

Somewhat to our surprise the raw data derived from a one filament model when plotted, approached most nearly the measured curve in an azimuth band of $0 \pm 60°$. The implication is that the inboard filaments are ineffective in the downward region; their effect is probably nullified by viscous mixing. To increase confusion there are regions where a two filament model appears to come off best; but detailed inspection of raw and smoothed output reveals that outside the downwind sector, the seven filament model with

variable circulation yields the best overall comparison. The saw-teeth in the raw profile are the least exaggerated and the smoothed contours approach more nearly the proportions of those deduced from the test cases. The suggestion of a further refinement was followed up in the form of a hybrid model confined to one tip vortex in a downwind sector, azimuth $0 \pm 45°$, but with full seven filament representation over the remainder of the disc. A distinct improvement in the comparison resulted (Figure 17). Discrepancies between

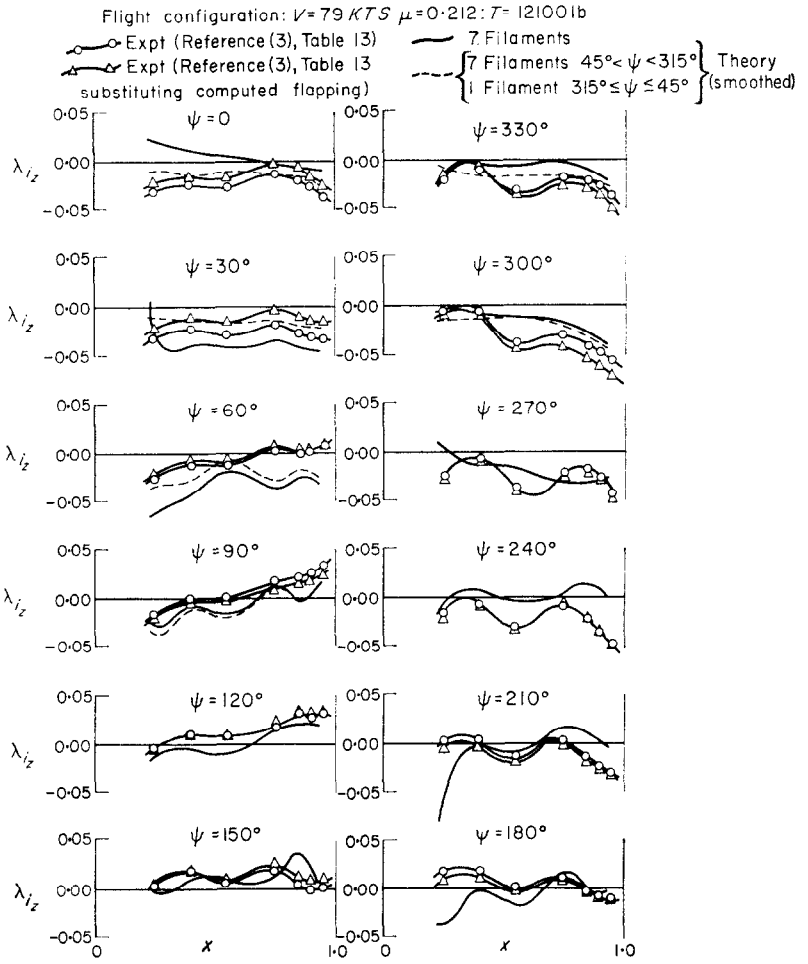

Figure 17. Downwash distribution—theory and experiment.

measured and calculated data are not necessarily due to deficiencies in a mathematical model, but can arise during processing of experimental results. In this instance, failure to take account of elastic deformation when interpreting test data has some bearing, but the effect of errors in rigid flapping is likely to be more important. A comparison between values tabulated in reference (3) and those calculated in the performance programme on a basis of downwash distribution deduced as described, revealed marked discrepancies with respect to coning angle. There was however close agreement in terms of integrated thrust, and arbitrating on this basis, the computed coning angle was shown to be more realistic. It was therefore decided to reprocess the flight data after substituting calculated for measured flapping angles. A second approximation so derived is, strictly speaking,

the next step of an iterative loop aimed at achieving consistency between downwash distribution and flapping history. No attempt has been made to continue the sequence, however, since indications are that it is rapidly convergent. The conclusion reached at this stage is that, although scope for refinement is by no means exhausted, near optimum potential of the simple model described has been exploited. A decision as to whether it is adequate for design purposes rests largely on the result of an intensive verification programme. Further improvements would almost certainly be sought in a more elaborate model.

In conjunction with the development of a suitable downwash model and during the later stages of this work, the first attempts were made to achieve consistent solutions of rotor performance, with downwash distribution related to blade loading, and parameters defining a realistic flight case. With an eye to an ultimate comparison, a typical case was chosen from reference (3). To make things a little more difficult, an equivalent Glauert downwash distribution was entered as a first approximation and a run made through the performance programme. The loop was closed, as illustrated in Figure 7, cycling through circulation processing, downwash distribution and downwash processing programs, back to the performance programme, and repeating the macro-cycle three times in all. In this preliminary attempt, blade motion, apart from feathering, was confined to rigid flapping, and downwash computed on a basis of uniform circulation using a seven filament model throughout and restricting wake age to one cycle of 360°, the main aim being an assessment of convergence characteristics. Figure 18 shows satisfactory progress generally, but with some sluggishness in the advancing blade region. Reluctance is most marked at azimuth 60°, an area well known for sensitivity to small changes of incidence. Following a tendency in that direction during the second cycle, there was a massive loss of thrust locally at the tip in the third, and only slight recovery in the fourth. The effect was traced to a tip vortex, issuing from blade number three, trailing close to the reference blade and generating a large downwash peak. The effect is realistic as its occurrence during successive cycles shows. Similar flight cases all display a downwash peak in this region, but less marked, and the exaggeration in this instance is attributed to some local peculiarity. No great significance is attached to such manifestations at an early stage of programme development except as pointers to possible refinements.

The main aim, to demonstrate the viability of the approach, appears to have been achieved. Although influenced adversely by this local sorespot, convergence in terms of blade load and downwash distribution, as well as integrated thrust and power, is rapid, and has encouraged us to undertake further development. Turning to the computed performance of the rotor, there are one or two interesting features worthy of comment. Comparing the output of the first with subsequent cycles, it can be seen that three distinct peaks have appeared on the profile tangential force curve. These are seen to be associated with peaks in the normal force component and are manifestations of incipient drag divergence. The generating mechanism is in the wake and is a function of advance ratio. As the blade passes through azimuth 60°, a march of tip vortices along its length commences and lasts until azimuth 290° (Figure 18). The effect is to generate regions of upwash which, through the agency of an increase in angle of attack, causes the critical Mach number to be exceeded locally. The result is a sharp drag rise. At around 90° the blade tip is thus affected, but at 240°, two widely separated vortices are each seen to generate a substantial area of drag divergence. The realism of the third peak at 330°, lying in the downwind sector, is suspect for reasons stated earlier. The powerful tip vortices have an even greater effect on the induced component of tangential force as is revealed most clearly when the blade is at 150° azimuth. The upwash field outboard of the vortex from blade number 1 is seen to cause a sharp rise in normal force gradient,

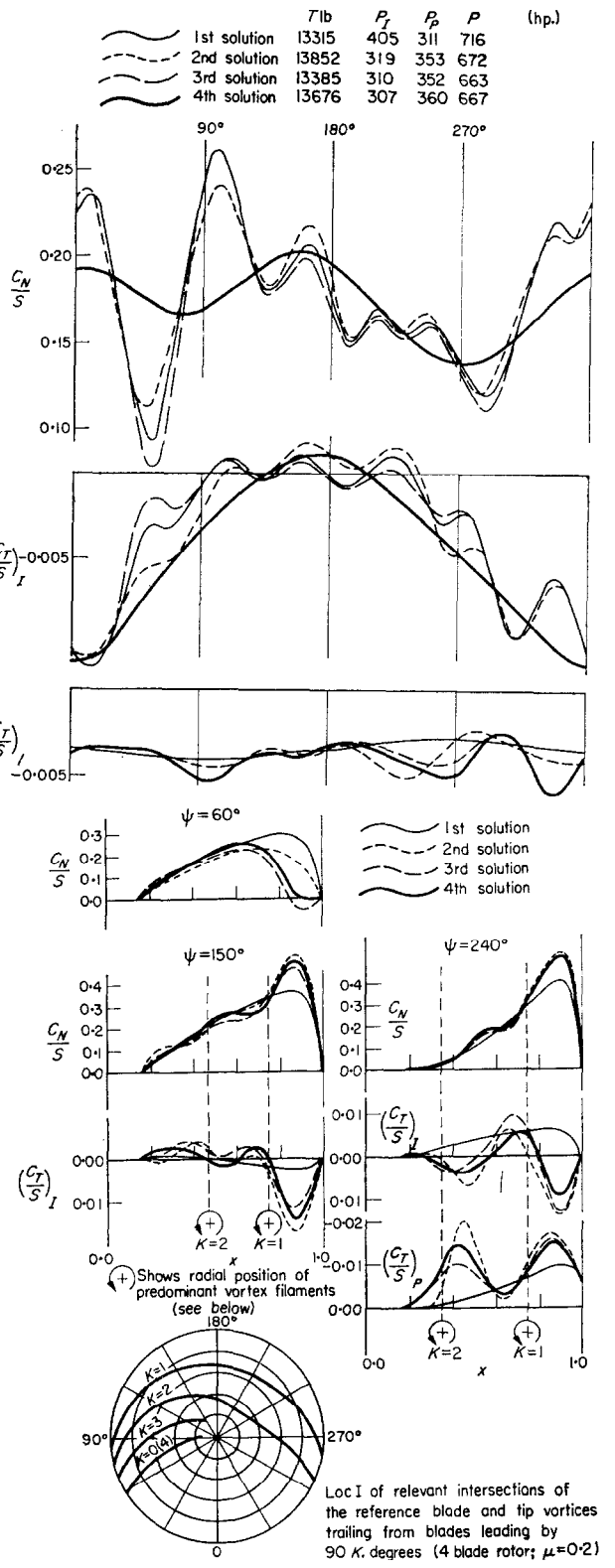

Figure 18. Rotor performance—convergent solution with non-uniform downwash.

generating a peak at the blade tip. In combination with upwash, a trough in the induced tangential force results. Two of these are evident, one for each vortex, the effect being yet more marked at 240° azimuth. The azimuthal distribution gives a clearer picture of two upwind regions symmetrically disposed about 180° in which there is a significant reduction of induced power, totalling some 100 hp. The effect, with reservations about the local trough at 330°, is thought to be wholly realistic, for Froude-Rankine momentum theory has long been known to seriously underestimate induced power in the minimum power speed band. To summarize, this new approach to performance estimation, as compared with more elementary methods, predicts drag divergence at a lower speed and computes appreciably reduced values of induced power. In this particular case, there is an overall reduction of the order of 50 hp, bringing the predicted figure more closely in line with flight test results.

To conclude, work has progressed to a stage where most programme material has been written and tested, but comparatively little has been done in the way of verification and application. There are therefore no firm conclusions.

ACKNOWLEDGMENTS

We would like to acknowledge the efforts of the rest of our colleagues who have contributed to the programme which is being carried out under contract to the Ministry of Aviation. Our thanks extend to those representatives of that ministry and to others outside Westland Aircraft organization whose co-operation has helped the programme on its way. Our thanks are also due to the Ministry of Aviation and our parent firm for permission to publish this paper, which nevertheless expresses our own opinions, not necessarily coinciding with those held by these authorities.

REFERENCES

1. J. M. HARRISON 1965 *Westland Aircraft Limited Technical Report Aero/Research/2.* Dynamics of a fully articulated rotor blade.
2. M. A. P. WILLMER 1963 *A.R.C. R & M* 3318. The loading of helicopter rotor blades in forward flight.
3. JAMES SCHEIMAN 1964 *NASA tech. Memor. X*-952. A tabulation of helicopter rotor blade differential pressures, stresses and motion as measured in flight.
4. PAUL J. CARPENTER 1958 *Tech. Notes natn advis. Comm. Aeronaut. Wash.* 4357. Lift and profile drag characteristics of an N.A.C.A. 0012 airfoil section as derived from helicopter-rotor hovering performance.
5. CRITZOS, HEYSON and BOSWINKLE Jr. 1955 *Tech. Notes natn advis. Comm. Aeronaut., Wash.* 3361. Aerodynamic characteristics of N.A.C.A. airfoil section at angles of attack from 0° to 180°.

APPENDIX

Notation

A_1, B_1 lateral and longitudinal components of cyclic pitch
a rotor blade section lift slope
b number of blades
C_L, C_D, C_N, C_T lift, drag, normal and tangential force section coefficients

$$C_{L,D}(\alpha, M) = \frac{L, D}{\frac{1}{2}\rho V_R^2 c\, dr},$$

$$\frac{C_N}{S} = (C_L \cos\phi + C_D \sin\phi)(\mu_T^2 + \mu_N^2),$$

$$\frac{C_T}{S} = (C_D \cos\phi - C_L \sin\phi)(\mu_T^2 + \mu_N^2)$$

C_{M_i} generalized moment acting on ith flatwise bending mode,

$$C_{M_i} \doteq \frac{\int_{e_a}^{R} F_N f_i \, dr}{\frac{1}{2}\rho c R^2 (\Omega R)^2}$$

c blade chord (ft)

$c_r(x)$, $s_r(x)$ polynomial Fourier coefficients of $\lambda_{i_z}(x,\psi)$ (smoothed),

$$\lambda_{i_z}(x, \psi) = c_0(x) + \sum_{r=1}^{6} \{c_r(x) \cos r\psi + s_r(x) \sin r\psi\}$$

where

$$c_r(x) = \sum_{n=0}^{6} c_{r_n} x^n, \quad s_r(x) = \sum_{n=0}^{6} s_{r_n} x^n$$

c_{r_n}, s_{r_n} coefficients of polynomials $c_r(x)$, $s_r(x)$

D drag force acting on blade element (lb)

e_a blade aerodynamic root offset from rotor centre (ft)

e_f offset of flapping hinge from rotor centre (ft)

F force component acting on blade element (lb)

$f_i(r)$ ith flatwise bending mode (ft)

I_B blade moment of inertia about flapping hinge (lb ft sec^2)

$I_{\beta\beta}$ 2nd moment of area about principal axis of flatwise bending (ft^4)

k blade number, κth blade leadsr eference blade by $\frac{2\pi k}{b}$

L lift force acting on blade element (lb)

M Mach number

M bending moment acting on blade element (lb ft)

$M(\beta_i)$ contribution of ith bending mode to bending moment (lb ft)

M_A aerodynamic pitching moment acting on blade element (lb ft)

m blade mass per unit length (slugs/ft)

N blade intersection solution counter (see Figure 8)

n number of bending modes admitted

P rotor horse power

R rotor radius

r radial displacement of blade element from rotor centre (ft)

s rotor solidity $= \frac{bc}{\pi R}$

T rotor thrust (lb)

V flight path velocity (ft/sec)

$V_{N,T}$ components of V_R : resolved normal and parallel to the xy plane

V_R air velocity component relative to blade element in plane normal to blade axis (ft/sec)

w_i induced velocity (ft/sec)

x, y, z aircraft body (shaft) axes, forces resolved along these axes (Figure 1)

X non-dimensional radial co-ordinate of blade element r/R

X_1 station of origin of trailing vortex filament (Figure 3)

X_2 blade/vortex intersection station (Figure 3)

Z non-dimensional displacement of wake element normal to tip path plane (Figure 5)

α blade element angle of attack

α_s angle of attack of xy-plane (Figure 1)

β blade flapping angle

β_i amplitude of ith normal mode (Figure 2)

γ_i generalized inertia coefficients $\gamma_i = \frac{\rho a c R^4}{R \int_{ef} m f_i^2 \, dr}$

δ angle between reference blade axis and rectangularized vortex (Figure 5)

ϑ blade geometric pitch angle

ϑ_0 blade pitch collective component

$\vartheta(r)$ blade twist distribution
λ_i induced velocity ratio $= w_i/\Omega R$
μ advance ratio $= V/\Omega R$
$\mu_{N,Tx}$ $V_N/\Omega R$, $V_T/\Omega R$ and $V\cos\alpha/\Omega R$, respectively
ϕ helix angle between V_R and xy plane
Ψ wake age parameter $= \frac{2\pi k}{b} - (\psi_1 - \psi)$
ψ azimuth angle measured from downwind blade position
ψ_1 azimuth angle of "ghost" blade; i.e., instantaneous blade azimuth at which vortex was shed (see Figure 3)
Ω rotor hub angular velocity about shaft axis ($\sec^{-1}$)
ω_i non-dimensional natural frequency of ith bending mode (Figure 2)

Subscripts

CR control rod
E edgewise component
F flatwise component
I induced component
N normal component
P profile component
T tangential component
x radial component or x-component
z component normal to tip-path plane

This paper was first presented at the Symposium on the Noise and Loading Actions of Helicopters, V/Stol Aircraft and Ground Effect Machines, September 1965 at the Institute of Sound & Vibration Research of the University of Southampton.